Journal of Biomechanics 84 (2019) 269–273

Contents lists available at ScienceDirect

Journal of Biomechanics

journal homepage: www.elsevier.com/locate/jbiomech
www.JBiomech.com

Short communication

Muscle volume reconstruction from several short magnetic resonance imaging sequences

Robert Marzilger, Arno Schroll, Sebastian Bohm, Adamantios Arampatzis *

Department of Training and Movement Sciences, Humboldt-Universität zu Berlin, Germany
Berlin School of Movement Sciences, Humboldt-Universität zu Berlin, Germany

ARTICLE INFO

Article history:
Accepted 19 December 2018

Keywords:
Muscle morphology
Vastus lateralis
Muscle volume
MRI

ABSTRACT

The gold standard to determine muscle morphological parameters is magnetic resonance imaging (MRI). To measure large muscles like the vastus lateralis (VL) in one sequence, scanners with a large field of view (FOV) and a high flux density are needed. However, large scanners are expensive and not always available. The purpose of the current study was to develop a marker-based approach to reconstruct the VL from several separate MRI sequences, acquired with a low-field MRI scanner. The VL muscle of 21 volunteers was marked at one-third and two-third of thigh length using fish oil capsules. Three consecutive MRI sequences (i.e. proximal, medial and distal part) of the thigh were captured between the markers and the muscle insertion and origin. After a manual segmentation of the VL the muscle was reconstructed using the developed approach. The muscle volume, maximal anatomical cross-sectional area and length were 715.1 ± 93.4 cm^3, 34.0 ± 4.0 cm^2 and 34.4 ± 2.2 cm respectively. The procedure showed an average error between 0.9% and 2.2% for the reconstructed muscle volume, the averaged RMSD between the cross-sectional areas of two overlapping sequences were between 0.80 ± 0.71 cm^2 and 0.88 ± 0.78 cm^2. The proposed approach provides an appropriate accuracy for muscle volume assessment, as the estimated error for muscle volume calculation was quite small. The reconstruction quality depends mainly on the proper marker attachment and identification, as well as the spatial resolution of the image sequences. We are confident that the presented method can be used in most investigations regarding muscle morphology.

1. Introduction

The measurement of muscle morphology (i.e. volume, anatomical cross-sectional area and length) is important in musculoskeletal research for the evaluation of training interventions (Blazevich et al., 2007; Vikne et al., 2006), the assessment of age-related muscle alterations (Mersmann et al., 2017; O'Brien et al., 2010) and the quantification of changes in muscle properties due to disease (Bland et al., 2011; Guler et al., 2016; Moreau et al., 2009). The gold standard methodology for the reconstruction of muscle morphology in vivo is based on magnetic resonance imaging (MRI) (Barber et al., 2009; Marcon et al., 2014; Walton et al., 1997). MRI is non-invasive, free of ionising radiation and provides high resolution images (Engstrom et al., 1991; Walton et al., 1997). The precise determination of muscle volume requires the reconstruction of the muscle by analyzing multiple MRI scans along a certain body axis (i.e. longitudinal axis) of the entire muscle.

Capturing large muscles like the vastus lateralis (VL) in a single MRI scan is only possible in high-field scanners providing a large field of view (FOV). However, high-field devices with a magnetic flux density above 1 Tesla (T) are rarely accessible (Schless et al., 2017) and mainly used in a clinical context. Therefore, low-field MRI scanners with a low magnetic flux density of 0.2–0.25 T and a small field of view have been alternatively used to determine muscle morphology for scientific purposes (Albracht et al., 2008; O'Brien et al., 2010; Seynnes et al., 2009). The financial costs of low-field scanners are substantially lower compared to high-field scanners (Coffey et al., 2013; Lee et al., 2015), however, a repositioning of the participants with respect to the FOV is needed to provide a sufficient number of images for a total reconstruction of large muscles like the VL.

From our perspective, the reconstruction of large muscles from several MRI sequences is the most crucial limitation when using small FOV scanners. Therefore, our purpose was to present a marker-based approach for a total reconstruction of a large muscle

* Corresponding author at: Humboldt-Universität zu Berlin, Department of Training and Movement Sciences, Philippstr. 13, Haus 11, 10115 Berlin, Germany.
E-mail address: a.arampatzis@hu-berlin.de (A. Arampatzis).

https://doi.org/10.1016/j.jbiomech.2018.12.038
0021-9290/

(i.e. VL) from three separate MRI sequences, acquired with a low-field and small FOV MRI scanner. The proposed methodology will enable researchers to reconstruct large muscles using small FOV MRI scanners.

2. Methods

2.1. Experimental design

MRI scans at three different sections of the thigh were taken from 21 male participants (age: 26.8 ± 4.6 y, height: 178.8 ± 6.5 cm, body mass: 73.2 ± 8.7 kg). All participants included in the study were informed about the aim and the measurement procedures and gave their written consent to participate in the investigation. The study was performed in accordance with the declaration of Helsinki and approved by the ethics board of the Humboldt-Universität zu Berlin.

2.2. Measurement

Prior to the MRI measurement the participant's thigh length was measured between the greater trochanter and the lateral epicondyle. The distance was separated in three segments and the segment borders were marked with a skin marking pen. At the two marks on the thigh elastic marker belts were attached accordingly (Fig. 1A). The marker belts consisted of elastic straps with three fish oil capsules. The fish oil capsules (from now on named marker) were later easy to identify in the image series, since they provide a bright signal in T1 weighted MRI sequences. Finally, the border of the marker belt was highlighted with the skin marking pen and secured at the participant's leg with tape. The procedures allowed to control and reduce the marker belts' movement during the necessary repositioning of the participants in the scanner throughout the measurement.

After the preparation, the participants were positioned supine in an open 0.25 Tesla MRI scanner (G-Scan, Esaote, Genua, Italy). First, the most proximal third of the thigh (proximal sequence) was scanned with 52 slices (Turbo 3D T1 weighted, TE: 16 ms, TR: 39 ms, slice thickness: 3.1 mm, no gaps). Afterwards the participants were repositioned in the scanner with respect to the FOV and the medial (medial sequence), followed by the distal (distal sequence) part of the thigh were scanned. The scanning settings for the medial and distal sequence were the same as we described before for the proximal sequence. During repositioning in the scanner, the position of the marker belt was carefully controlled to avoid any potential movement. In all measurements, we took care that at least one marker was completely visible in either of the two consecutive scanned sequences.

2.3. Muscle reconstruction

In the captured image sequences the border of the VL muscle was manually identified in every slice using the software Osirix (version 4.0, Pixmeo, Geneva, Swiss), segmenting precisely the inner layer of the epimysium (Fig. 1B). Care was taken that at least an overlap of three slices for two subsequent sequences (i.e. proximal-medial and medial-distal) was digitized. The three markers were manually identified in each image sequence. Although in some cases only a part of a marker was visible within a sequence, in the most cases the fish oil capsules were visible in their entire length (i.e. each marker was visible for 8 to 10 consecutive slices). Fig. 1B provides an MRI image with the identified VL and the markers in the proximal and medial scanning sequence of the thigh at the same longitudinal position (i.e. overlapping region). The analyzed sequences were post-processed using a custom written Matlab (2012, The Mathworks, Natick, USA) algorithm for the connected sequences (i.e. proximal-medial sequence and medial-distal sequence).

In a first step, the algorithm calculated the shift in the z-direction (i.e. longitudinal axis of the MRI scanner) between two consecutive sequences using the identified markers. For each marker that was completely visible (being present in at least eight slices) and segmented, the necessary shift of the more distal sequence was calculated to superimpose the corresponding marker in the more proximal sequence along the longitudinal axis (i.e. the proximal end of a marker being in the same z-level in both

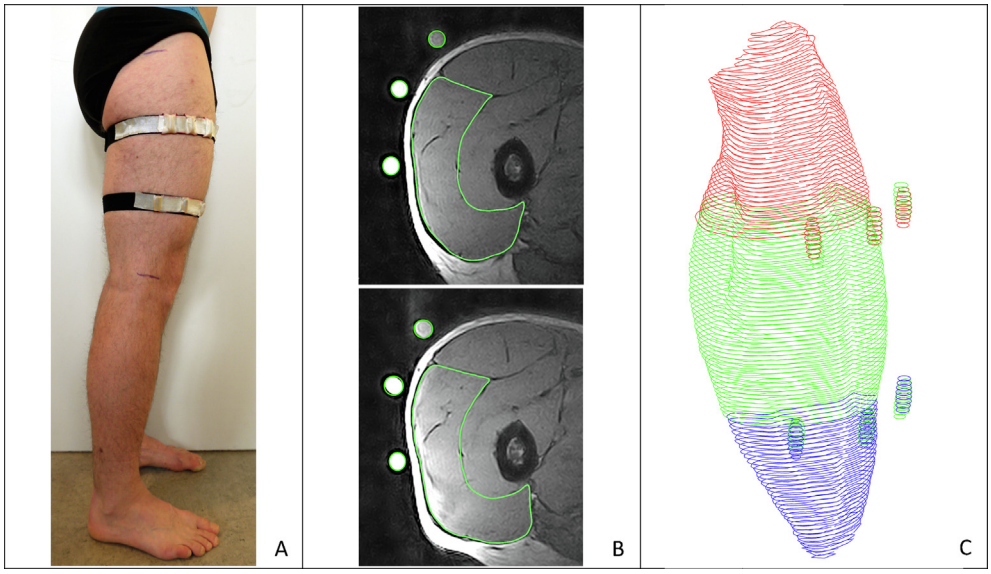

Fig. 1. Process of muscle reconstruction from the participants' preparation (A), manual vastus lateralis segmentation (B) and model of the reconstructed muscle (C). Image A shows the elastic straps with the fish oil capsules attached to the leg. Image B shows approximately the same identified part of the muscle and the fish oil capsules in a slice in the proximal (top) and medial (bottom) muscle segment. Image C shows a model of the fully reconstructed muscle with its proximal (red), medial (green) and distal (blue) parts on the basis of the respective digitized fish oil capsules. (For interpretation of the references to colour in this figure legend, the reader is referred to the web version of this article.)

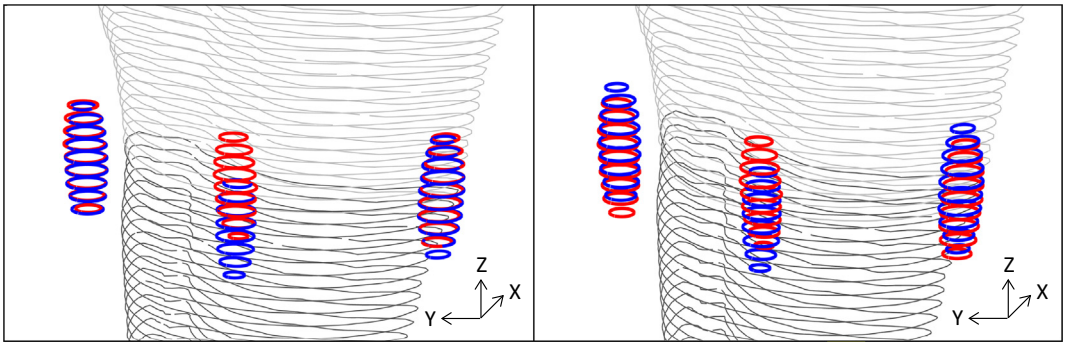

Fig. 2. Example of the procedure of the MRI sequence shift in the Z-direction (i.e. longitudinal axis of the MRI scanner) with respect to the contributing slices of the markers in two connected sequences. The left image shows the sequence before the shift and the right image thereafter. To improve visibility, the rotation and translation of the more proximal part (second step of the reconstruction process) were already applied in the left image. Before the shift the left marker is visible in the same relative slices in the proximal (red) and distal (blue) sequence (zero offset). For the middle marker the proximal and the distal part show an offset of three slices between the sequences. For the right marker the offset between both sequences is one slice. Hence the total offset is 4/3 slices (4 slices by 3 markers). Consequently the distal part is shifted by 4/3 of the slice thickness in the direction toward the more proximal part. (For interpretation of the references to colour in this figure legend, the reader is referred to the web version of this article.)

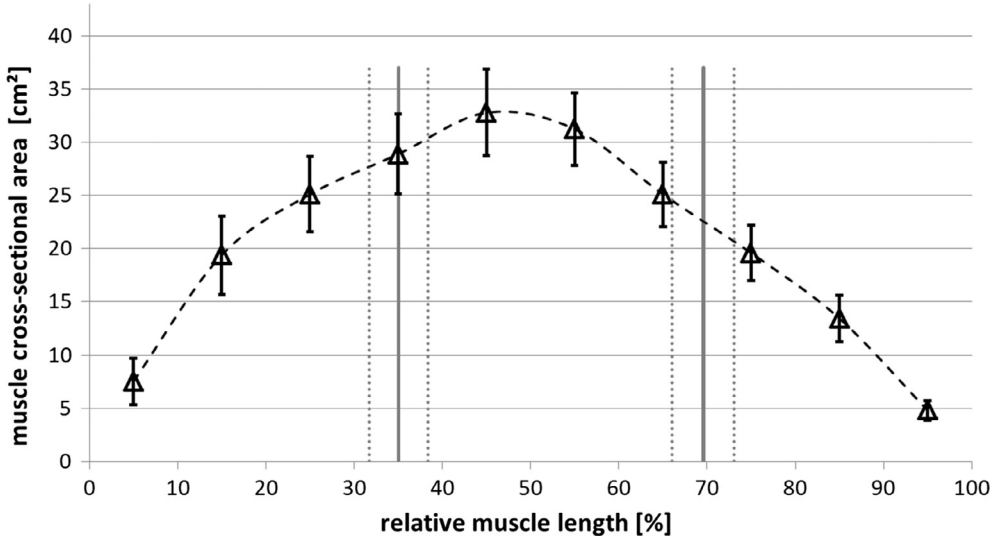

Fig. 3. Average muscle anatomical cross-sectional area and standard deviation (error bars) along the muscle length. Values were calculated in 10% intervals from the proximal to the distal part of the muscle. The vertical lines indicate the mean (solid grey lines) and standard deviation (dashed grey lines) of the position of the overlapping areas of the proximal-medial (left) and medial-distal (right) MRI sequences.

sequences). The resultant shift of the sequence was calculated as the average shift of the individual markers. Details of the procedure are presented exemplary in Fig. 2. The accuracy of the marker length identification and the resultant shift calculation is affected by the resolution in the z-direction (i.e. slice thickness). With a lower resolution, it is more likely that the real marker endpoints are between two slices and not in a scanned image. In consequence, the identified markers' endpoints may introduce an inaccuracy of one slice thickness. This potential error was reduced by allowing an additional shift between the two sequences by plus/minus one slice in either direction. The allowed additional shift was calculated using a least square approach that minimized the squared differences in muscle anatomical cross-sectional area (ACSA) in the overlapping parts.

After the shift of the two consecutive sequences in the z-direction, we determined the rotation around the z-axis and the translation in the transverse plane (i.e. x-y plane) between two scanning sequences. A transformation matrix T was calculated using homogenous coordinates to describe the rotation and translation of the distal in relation to the proximal sequence in the transverse plane. First, the geometrical centers (c) of the identified markers in the transverse plane of both sequences were represented in homogenous coordinates, particularly $c_i^1 = (x_i^1 \quad y_i^1 \quad 1)'$ for the more proximal part and $c_i^2 = (x_i^2 \quad y_i^2 \quad 1)'$ for the more distal part with $i \in \{1, \cdots, 3\}$. Then the transformation matrix $T = \begin{pmatrix} R & t_x \\ 0 \quad 0 & t_y \\ & 1 \end{pmatrix}$ with a 2D rotation matrix R and a translation $t = (t_x, t_y)$, was determined using constrained optimization to minimize the squared distances between c_i^1 and $T \cdot c_i^2$. The optimization constraint was that the determinant of the rotation matrix R needs to be one. Lastly, the distal sequence was transformed using the matrix T to superimpose over the proximal sequence in the overlapping region. Finally, after the two reconstruction steps the muscle volume was calculated by integrating the ACSA along the z-axis with the trapezoidal rule. The steps from the participant preparation to the final muscle volume reconstruction are shown in Fig. 1A–C.

From the reconstructed muscle we determined volume, maximal cross-sectional area ($ACSA_{max}$) and length of the VL muscle. We calculated the probable error in the reconstructed

Table 1
Estimated effect of possible errors in muscle sequence overlap on the whole muscle volume (715.1 ± 93.4 cm^3) calculation. The error is calculated with regard to the average muscle cross-sectional area at the overlapping region under the assumption of an overlap of one slice between two sequences (the equations for error calculation are given in the methods section). Results are shown for the proximal-medial and medial-distal sequence separately and as the sum of both overlapping regions.

Proximal-medial sequence		Medial-distal sequence		Sum of both overlapping regions	
Absolute error [cm^3]	Relative error [%]	Absolute error [cm^3]	Relative error [%]	Absolute error [cm^3]	Relative error [%]
8.9	1.2	6.7	0.9	15.6	2.2

muscle volume for one slice overlap between two sequences using the following equations: $probable\ volume\ error = \frac{volume\ at\ overlap}{total\ muscle\ volume}[\cdot 100\%]$ and $volume\ at\ overlap = ACSA_{avg} \cdot erroneous\ slices\ at\ overlap \cdot slice\ thickness$, with $ACSA_{avg}$ as the average cross-sectional area at sequence overlap. In addition, the root mean square deviation $RMSD = \sqrt{\frac{\sum_{i=1}^{n}(ACSA_{1,i} - ACSA_{2,i})^2}{n}}$ between the cross-sectional areas of two overlapping sequences was calculated. With $ACSA_1$ and $ACSA_2$ being the cross-sectional areas in the overlapping region (e.g. proximal and medial) and n the number of overlapping slices.

3. Results

The average muscle volume, $ACSA_{max}$ and length were 715.1 ± 93.4 cm^3, 34.0 ± 4.0 cm^2 and 34.4 ± 2.2 cm respectively. The average position of the overlapping region, in respect to the muscle length was at 35.3 ± 3.3% from the proximal to medial sequence and at 70.0 ± 4.0% from the medial to distal sequence (Fig. 3). The average ACSA at the proximal to medial sequence overlap was 28.9 ± 4.6 cm^2 and 21.7 ± 3.6 cm^2 at the medial to distal overlap. The average error in muscle volume was between 0.9% and 2.2% for an error of one slice in the overlapping regions (Table 1). The averaged RMSD between the areas of the two sequences was 0.80 ± 0.71 cm^2 at the proximal to medial sequence and 0.88 ± 0.78 cm^2 at the medial to distal sequence (i.e. 2.8% and 4.0% respectively).

4. Discussion

In the current study we provided a methodological approach to reconstruct the entire VL muscle from several connected MRI sequences of a low-field, small FOV MRI scanner. The calculated VL muscle volumes were similar to literature reports using large field of view scanners (Mersmann et al., 2015; O'Brien et al., 2009). Furthermore, the estimated error of the proposed method was approximately 2% for the whole VL muscle volume reconstruction. Therefore, the presented method can be used without relevant limitations for the assessment of muscle morphology.

The expected changes in the VL muscle volume after training interventions are higher than 10% (Blazevich et al., 2007) and, therefore, well detectable with the proposed approach. Similarly, the reported differences in VL muscle volume due to disease (Hart et al., 2012) or aging (O'Brien et al., 2010) are higher than 10%, which supports the applicability of the proposed methodology in cross-sectional studies too. The small error in volume assessment can be attributed to the small slice thickness (e.g. 3.1 mm) in the MRI scanning, which resulted in a high spatial measurement accuracy. Furthermore the high spatial resolution in combination with the small estimated number of erroneous overlapping slices (±1) resulted in a rather low error of 0.9–2.2% (Table 1) in the overlapping regions (CSA × slice thickness) to the total muscle volume. This was despite the large ACSA of 84.3% (proximal-medial) and 63.9% (medial-distal) of the $ACSA_{max}$ in the overlapping regions. Moreover, the RMSD between the areas in the overlapping regions was 2.8% between the proximal and medial sequence and 4% between the medial and distal sequence, giving almost identical area sizes in the overlapping regions after the transformation.

Using the presented approach, the error in muscle length determination is ±1 slice at the insertion and origin of the muscle due to the spatial resolution of the MRI measurement and an additional ±1 slice at the overlapping regions. However, the spatial resolution is a general issue of the MRI methodology and not related to the proposed approach. The possible error induced at the two overlapping regions of ±6.2 mm (2 × 3.1 mm slice thickness) is within (Maden-Wilkinson et al., 2014; Marcon et al., 2014; O'Brien et al., 2009) or below (Blazevich et al., 2007; Ogawa et al., 2012; Vikne et al., 2006) the slice thickness (i.e. measurement error) of other investigations. Accordingly, a larger slice thickness or inter slice gaps can result in a larger error in the muscle length determination due to improper identification of the muscles' insertion and origin in the MRI sequence (spatial resolution). Hence, it is reasonable to argue that the small slice thickness (with no gaps) and the high accuracy of the sequence composition in our approach ensured that the possible error in muscle length from the overlapping regions is marginal.

5. Conclusion

The developed algorithm reconstructed the muscle volume from three different MRI scans on the basis of manually identified external markers (fish oil capsules) within the scans. The reconstruction quality depends mainly on the proper marker attachment and identification, as well as high spatial resolution (small slice thickness and no gaps). With the proposed method we were able to accurately reconstruct the VL muscle and calculate volume, $ACSA_{max}$ and length, from three connected MRI sequences captured with a small FOV scanner. Hence, the method allows using small FOV MRI scanners for the assessment of the morphology of large muscles.

Conflict of interest

The authors declare no conflict of personal or financial interests.

Acknowledgement

This work was supported by the Federal Institute of Sport Science (BISp) Germany [ZMVI1-070108/14-16]; and the foundation Stiftung Oskar-Helene-Heim.

References

Albracht, K., Arampatzis, A., Baltzopoulos, V., 2008. Assessment of muscle volume and physiological cross-sectional area of the human triceps surae muscle in vivo. J. Biomech. 41, 2211–2218. https://doi.org/10.1016/j.jbiomech.2008.04.020.

Barber, L., Barrett, R., Lichtwark, G., 2009. Validation of a freehand 3D ultrasound system for morphological measures of the medial gastrocnemius muscle. J. Biomech. 42, 1313–1319. https://doi.org/10.1016/j.jbiomech.2009.03.005.

Bland, D.C., Prosser, L.A., Bellini, L.A., Alter, K.E., Damiano, D.L., 2011. Tibialis anterior architecture, strength and gait in individuals with cerebral palsy. Muscle Nerve 44, 509–517. https://doi.org/10.1002/mus.22098.

Blazevich, A.J., Cannavan, D., Coleman, D.R., Horne, S., 2007. Influence of concentric and eccentric resistance training on architectural adaptation in human quadriceps muscles. J. Appl. Physiol. 103, 1565–1575. https://doi.org/10.1152/japplphysiol.00578.2007.

Coffey, A.M., Truong, M.L., Chekmeney, E.Y., 2013. Low-field MRI can be more sensitive than high-field MRI. J. Magn. Reson. 237, 169–174. https://doi.org/10.1519/JSC.0b013e3181b86712.Youth.

Engstrom, C.M., Loeb, G.E., Reid, J.G., Forrest, W.J., Avruch, L., 1991. Morphometry of the human thigh muscles. A comparison between anatomical sections and computer tomographic and magnetic resonance images. J. Anat. 176, 139–156.

Guler, O., Mahirogullari, M., Isyar, M., Piskin, A., Yalcin, S., Mutlu, S., Sahin, B., 2016. Comparison of quadriceps muscle volume after unilateral total knee arthroplasty with and without tourniquet use. Knee Surgery, Sport. Traumatol. Arthrosc. 24, 2595–2605. https://doi.org/10.1007/s00167-015-3872-5.

Hart, H.F., Ackland, D.C., Pandy, M.G., Crossley, K.M., 2012. Quadriceps volumes are reduced in people with patellofemoral joint osteoarthritis. Osteoarthr. Cartil. 20, 863–868. https://doi.org/10.1016/j.joca.2012.04.009.

Lee, R.K.L., Griffith, J.F., Lau, Y.Y.O., Leung, J.H.Y., Ng, A.W.H., Hung, E.H.Y., Law, S.W., 2015. Diagnostic capability of low-versus high-field magnetic resonance imaging for lumbar degenerative disease. Spine (Phila. Pa. 1976). 40, 382–391. https://doi.org/10.1097/BRS.0000000000000774.

Maden-Wilkinson, T.M., McPhee, J.S., Rittweger, J., Jones, D.A., Degens, H., 2014. Thigh muscle volume in relation to age, sex and femur volume. Age (Omaha) 36, 383–393. https://doi.org/10.1007/s11357-013-9571-6.

Marcon, M., Ciritsis, B., Laux, C., Nanz, D., Nguyen-Kim, T.D.L., Fischer, M.A., Andreisek, G., Ulbrich, E.J., 2014. Cross-sectional area measurements versus volumetric assessment of the quadriceps femoris muscle in patients with anterior cruciate ligament reconstructions. Eur. Radiol. 25, 290–298. https://doi.org/10.1007/s00330-014-3424-2.

Mersmann, F., Bohm, S., Schroll, A., Boeth, H., Duda, G., Arampatzis, A., 2015. Muscle shape consistency and muscle volume prediction of thigh muscles. Scand. J. Med. Sci. Sport. 25, e208–e213. https://doi.org/10.1111/sms.12285.

Mersmann, F., Bohm, S., Schroll, A., Boeth, H., Duda, G.N., Arampatzis, A., 2017. Muscle and tendon adaptation in adolescent athletes: a longitudinal study. Scand. J. Med. Sci. Sport. 27, 75–82. https://doi.org/10.1111/sms.12631.

Moreau, N.G., Teefey, S.A., Damiano, D.L., 2009. In vivo muscle architecture and size of the rectus femoris and vastus lateralis in children and adolescents with cerebral palsy. Dev. Med. Child Neurol. 51, 800–806. https://doi.org/10.1111/j.1469-8749.2009.03307.x.

O'Brien, T.D., Reeves, N.D., Baltzopoulos, V., Jones, D.A., Maganaris, C.N., 2010. Muscle-tendon structure and dimensions in adults and children. J. Anat. 216, 631–642. https://doi.org/10.1111/j.1469-7580.2010.01218.x.

O'Brien, T.D., Reeves, N.D., Baltzopoulos, V., Jones, D.A., Maganaris, C.N., 2009. Strong relationships exist between muscle volume, joint power and whole-body external mechanical power in adults and children. Exp. Physiol. 94, 731–738. https://doi.org/10.1113/expphysiol.2008.045062.

Ogawa, M., Yasuda, T., Abe, T., 2012. Component characteristics of thigh muscle volume in young and older healthy men. Clin. Physiol. Funct. Imaging 32, 89–93. https://doi.org/10.1111/j.1475-097X.2011.01057.x.

Schless, S.-H., Hanssen, B., Cenni, F., Bar-On, L., Aertbeliën, E., Molenaers, G., Desloovere, K., 2017. Estimating medial gastrocnemius muscle volume in children with spastic cerebral palsy: a cross-sectional investigation. Dev. Med. Child Neurol. I 81–87. https://doi.org/10.1111/dmcn.13597.

Seynnes, O.R., Erskine, R.M., Maganaris, C.N., Longo, S., Simoneau, E.M., Grosset, J.F., Narici, M.V., 2009. Training-induced changes in structural and mechanical properties of the patellar tendon are related to muscle hypertrophy but not to strength gains. J. Appl. Physiol. 107, 523–530. https://doi.org/10.1152/japplphysiol.00213.2009.

Vikne, H., Refsnes, P.E., Ekmark, M., Medbo, J.I., Gundersen, V., Gundersen, K., 2006. Muscular performance after concentric and eccentric exercise in trained men. Med. Sci. Sport. Exerc. 38, 1770–1781. https://doi.org/10.1249/01.mss.0000229568.17284.ab.

Walton, J.M., Roberts, N., Whitehouse, G.H., 1997. Measurement of the quadriceps femoris muscle using magnetic resonance and ultrasound imaging. Br. J. Sports Med. 31, 59–64. https://doi.org/10.1136/bjsm.31.1.59.